The projected poleward shift of tropical cyclogenesis at a global scale under climate change in MRI-AGCM3.2H

Xi Cao[1, 2]*, Masahiro Watanabe[2], Renguang Wu[3], Wen Chen[4], Ying Sun[5], Qing Yan[6], Pengfei Wang[1], Difei Deng[7] and Liang Wu[1]

[1]*Center for Monsoon System Research, Institute of Atmospheric Physics, Chinese Academy of Sciences, Beijing, China*

[2]*Atmosphere and Ocean Research Institute, University of Tokyo, Chiba, Japan*

[3]*School of Earth Sciences, Zhejiang University, Hangzhou, China*

[4]*Department of Atmospheric Science, Yunnan University, Kunming, China*

[5]*National Climate Center, China Meteorological Administration, Beijing, China*

[6]*Nansen-Zhu International Research Centre, Institute of Atmospheric Physics, Chinese Academy of Sciences, Beijing, China*

[7]*School of Science, University of New South Wales, Canberra, Australia*

Geophysical Research Letters

Submitted on September 13, 2023

Revised on November 7, 2023

Revised on December 5, 2023

Revised on January 17, 2024

Accepted on January 21, 2024

Correspondence to: Dr. Xi Cao. Institute of Atmospheric Physics, Chinese Academy of Sciences, Beichen West Road 81, Beijing, China

Email: caoxi09@mail.iap.ac.cn

Key points:

- We project a global feature of the robust poleward shift of TC genesis during active seasons of both hemispheres.
- More TC genesis at high latitudes can be attributed to the weakening of the Hadley circulation.
- Poleward shift of TC genesis emerges at 2K warming over Arabian Sea, South Atlantic and Pacific Oceans and at 4K warming over North Pacific.

Abstract

Future climate projections suggest a poleward shift of the maximum intensity of tropical cyclones (TCs) over the western North Pacific. However, the global nature of the latitudinal change in TC genesis under global warming remains poorly understood. We show, using large-ensemble high-resolution atmospheric model simulations (d4PDF) with four warming scenarios, that the poleward shift is a robust change over the globe, attributable to the weakening of the Hadley circulation. The weakened ascent driven by the upper-tropospheric warming suppresses the TC genesis within 5°-20° latitudes, whereas the weakened descent enhances the TC genesis in the poleward latitudes. We further estimate the poleward shift of TC genesis to emerge at the 2 K global warming over the Arabian Sea, South Atlantic and Pacific Oceans and at the 4 K warming over the North Pacific. The present results underscore the potential for increasing social and economic risks associated with TCs at higher latitudes.

Keywords: TC genesis; poleward shift; time of emergence; global warming.

Plain Language Summary

Climate models have projected a decrease in TC genesis frequency in future warming. However, the global nature of the latitudinal change in TC genesis under global warming remains uncertain partly due to insufficient resolution as well as the ensemble size of climate model simulations. We show a global feature of the robust poleward shift of the TC genesis during the active seasons of both hemispheres scaled with the global warming level, which can be attributed to the weakening of the Hadley circulation. The weakened ascending branch of the Hadley circulation, driven by the increased upper tropospheric warming, potentially hinders TC genesis within 5°-20° latitudes. Conversely, the weakened descending branch of the Hadley circulation enhances the likelihood of TC genesis within 20°-35° latitudes. We further estimate that the signal of TC genesis is expected to emerge over high latitudes of the Arabian Sea, South Atlantic and South Pacific Oceans at the 2 K warming and at the 4 K warming over the North Pacific. The present analyses have significant implications not only for assessing the reliability of future TC-related changes in climate models but also for estimating the increased TC-related hazards at higher latitudes under global warming.

1. Introduction

The impact of future global warming on tropical cyclone (TC) activity is highly intriguing not only scientifically but also socioeconomically because of the potential implications for loss and damage associated with climate change. Numerous studies have investigated the future changes in TC activity, encompassing metrics such as genesis and occurrence frequencies, intensity, and rainfall, using global and regional climate models (Allen & Ingram, 2002; Knutson et al., 2015; Li et al., 2010; Nakamura et al., 2017; Sugi et al., 2002; Sobel et al., 2016). Previous studies have revealed a consensus regarding the amplification in TC intensity and precipitation with anthropogenic warming (Knutson et al., 2020). However, there is a low degree of confidence and a lack of consensus regarding changes in TC genesis frequency and location under global warming, contributing to the overall uncertainty in assessing the comprehensive effects of climate change on TC activities (Knutson et al., 2020). This highlights the ongoing need for further research toward a deeper understanding of the complex relationship between global warming and TC activity.

Numerous previous studies have consistently shown a decline in global TC genesis number in response to greenhouse warming based on various climate models employing different resolutions or future emission scenarios (Sugi et al., 2009, 2015; Tory et al., 2013; Wehner et al., 2018; Zhao et al., 2009). Two hypotheses are proposed to explain the underlying mechanisms for this decrease but uncertainty still remains (Knutson et al., 2010, 2020; Seneviratne et al., 2021). One hypothesis links it to the increase in moist saturation deficit in the free troposphere (Emanuel et al., 2008), while the other relates it to the reduction in upward mass flux due to increased upper-tropospheric stability (Held

& Soden, 2006; Sugi et al., 2002, 2012; Zhao et al., 2013). However, several studies have also projected an increase in global TC genesis frequency (Emanuel, 2013; Bhatia et al., 2018). .

Given the relatively low genesis frequency and substantial internal variability of TCs, conducting large-ensemble simulations is crucial for exploring the comprehensive probability distribution of TC activity in future warming (Yoshida et al., 2017). An extensive 5000-year large-ensemble simulation (Mizuta et al., 2017), known as the database for Policy Decision making for Future climate change (d4PDF), is conducted using a 60-km atmospheric general circulation model under different warming scenarios. Previous studies have demonstrated that the d4PDF simulation exhibits a good skill in replicating the observed interannual-interdecadal large-scale atmospheric circulation variability linked to global sea surface temperature (SST) variation and TC genesis frequency (Kamae et al., 2017; Mizuta et al., 2017; Mei & Li, 2022; Ueda et al., 2018; Yoshida et al., 2017). These results motivate us to utilize the d4PDF dataset for capturing the essential features of TC activity and its connection with the prevailing large-scale atmospheric conditions under global warming.

Previous research has projected a poleward shift of the latitude of maximum TC intensity over the western North Pacific (Kossin et al., 2016), as well as projected an expansion in either poleward or eastward direction of TC occurrence frequency over the North Pacific (Knutson et al., 2020). However, research on the potential change in TC genesis locations under global warming has been relatively limited. Recent observational studies have identified a poleward shift of TC genesis, which is linked to the Hadley cell expansion (Daloz & Camargo, 2018; Sharmila & Walsh, 2018). This raises one question

of whether this poleward migration of TC genesis will continue under global warming and whether the Hadley cell expansion can explain the projected poleward shift. Our analyses of the d4PDF data demonstrate a robust poleward shift in global TC genesis locations under +4 K warming. However, the projected poleward shift of TC genesis cannot be solely explained by the Hadley cell expansion. Therefore, the objective of this study includes the investigation of the underlying physical mechanisms responsible for the poleward migration in global TC genesis locations under global warming as well as the determination of the time of emergence for this poleward shift in six regions that represent the global TC activity.

2. Data and methods

2.1. Observational TC data and domain of TC genesis

The observational TC geneses around the globe are portrayed by the best-track data from the International Best Track Archive for Climate Stewardship (IBTrACS), maintained by the National Centers for Environmental Information, National Oceanic and Atmospheric Administration (Knapp et al., 2010). The TC dataset comprises the TC location with latitude and longitude coordinates and the corresponding maximum sustained wind speed every six hours. The TC genesis in the IBTrACS dataset is determined as the initial time when a TC's maximum wind speed exceeds a threshold intensity of 34 knots, which is equivalent to approximately 17 m s^{-1}. For this study, we utilize the TC best track data from 1979 to 2010 to maintain consistency with the d4PDF dataset.

Our analysis concentrates on the global TC genesis during their respective TC peak seasons: from July to October (JASO) in the Northern Hemisphere (NH) and from January to April (JFMA) in the Southern Hemisphere (SH). The NH and SH regions include areas between 40 °E and 350 °E. Additionally, our analysis considers six individual basin oceans (Supplementary Fig. 1): the western North Pacific (WNP, 100 °-180 °E, north of the equator), the eastern North Pacific (180 °-285 °E, north of the equator), the northern Indian Ocean (NIO, 50 °-100 °E, north of the equator), the northern Atlantic Ocean (NAO, 260 °-350 °E, north of the equator), the southern Indian Ocean (SIO, 30 °-100 °E, south of the equator) and the southern Pacific Ocean (SPO, 150 °-230 °E, south of the equator). Note that for the NIO, the TC active season typically spans from April to June and from September to December (Li et al., 2013). However, for the sake of consistency with other regions, our analysis still focuses on the period of JASO. Meantime, the results over the NIO in JASO is similar to that from September to December.

2.2. Simulation data

In the present study, we utilize the d4PDF dataset, a comprehensive large-ensemble simulation dataset for past, current, and future climates, generated by the atmospheric general circulation model of Meteorological Research Institute of Japan (MRI-AGCM3.2H) (Mizuta et al., 2017). Previous studies have indicated that the single-model large ensemble is a valuable measure for quantifying and separating internal climate variability and the model's responses to changes in external forcings (e.g., Deser

et al., 2012; Maher et al., 2021; Milinski et al., 2020; Mizuta et al., 2017). In addition, the value of the single-model large ensembles is also from identifying and sampling extremes events, despite their low probability of occurrences (Haugen et al., 2018; Maher et al., 2021). The long-term simulation dataset is readily accessible online via https://diasjp.net/en/. The horizontal resolution of the model is set at a grid spacing equivalent to 60 kilometers, with the model top positioned at 0.01 hPa.

For the current historical climate simulation, referred to as HST, there is a 60-year integration spanning from 1951 to 2010. The simulation is driven by observed SST and sea ice concentration data from COBE-SST2 (Hirahara et al., 2014) as well as observed greenhouse gas concentrations. The HST simulation comprises 100 ensemble members, employing perturbations in the initial atmospheric conditions and monthly SST anomalies (Supplementary Table 1).

The past climate simulation, denoted as NWA, is similar to HST run, but with the removal of the long-term trend. This assumes a preindustrial climate without global warming. The NWA simulation also comprises 100 ensemble members, employing the identical initial and boundary conditions as the HST run. The reference point for detrended SSTs is established as the mean from 1900 to 1919, while greenhouse gas concentrations are set to estimated values in 1850.

For the future climate simulations, labeled as W2K and W4K, 60-year runs are conducted with a constant warming condition representing the approximate levels of the

year 2040 and 2090, respectively, in the Representative Concentration Pathway 8.5 (RCP8.5) scenario adopted in CMIP5. In these simulations, six climatological SST warming patterns are incorporated into the observed SST pattern while removing the long-term trend components. Each pattern is scaled to reproduce a global-mean surface air temperature increase of 2 K and 4 K, respectively. The W2K and W4K runs consist of a total of 54 and 90 ensemble members, respectively, grounded on the six future SST patterns and their associated perturbations. Further details on the experimental design can be found in the previous studies (Fujita et al., 2019; Mizuta et al., 2017). Note that our analysis is centered on the most recent 32 years of each climate simulation.

The TC tracking method employed in this study as well as the threshold values utilized align with the approaches described in the previous research (Murakami et al., 2012a; Yoshida et al., 2017). For more specific information, we refer readers to their studies. The TC genesis and TC track data are converted into a $5° \times 5°$ grid box through interpolation in order to calculate the climatological mean pattern and difference pattern.

2.3. Moist saturation deficit

The mid-tropospheric moisture content is quantified using the moist saturation deficit (χ) parameter, which is defined in accordance with the previous research (Emanuel et al., 2008; Yan et al., 2019; Emanuel 2013;):

$$\chi = \frac{s^* - s_m}{s_0^* - s^*}, \quad (1)$$

$$s = c_p log(T) - R_d log(p_d) + \frac{L_{vo} r_v}{T} - R_v r_v log(RH), \quad (2)$$

where s^* and s_0^* represent the moist entropies saturated at 600 hPa and sea surface, respectively, and s_m represents the moist entropy at 600 hPa, T represents the temperature, r_v represents the mixing ratio, p_d represents the partial pressure of dry air, RH represents the relative humidity, and the remaining parameters are held constant. A larger value of χ denotes a greater deficit in the mid-tropospheric moisture content, indicating an environment that is less favorable for TC genesis.

2.4. Dynamical genesis potential index

The dynamic genesis potential index (DGPI) is a metric utilized to assess the collective effects of various environmental parameters on TC genesis (Wang & Murakami, 2020). Wang & Murakami (2020) found that the DGPI is more skillful to represent the interannual variation of TC genesis over most of the basins compared to the original GPI developed by Emanuel and Nolan (2004). Recently, Wang et al. (2023) found a significant positive correlation between DGPI and TC genesis, which suggests a better representation in the decadal variability of TC genesis over the western North Pacific compared to the original GPI. The index is calculated as follows:

$$DGPI = (2 + 0.1V_{shear})^{-1.7} \times (5.5 - \frac{\partial u}{\partial y}10^5)^{2.3} \times (5 - 20\omega)^{3.4} \times (5.5 + |10^5\eta|)^{2.4} \times e^{-11.8} - 1, \quad (3)$$

where V_{shear} represents the magnitude of the vertical wind vector difference between 200 hPa and 850 hPa (m s^{-1}), $\frac{\partial u}{\partial y}$ represents the meridional gradient of zonal wind at 500 hPa

(s^{-1}), ω represents the 500-hPa vertical p-velocity (Pa s^{-1}), and η represents the 850-hPa absolute vorticity (s^{-1}).

2.5. Hadley circulation

The Hadley circulation is often studied using the Stokes streamfunction (ψ) in the assumption of a non-divergence meridional circulation. The Stokes streamfunction (ψ) is a frequently utilized variable for assessing the magnitude and extent of the Hadley circulation. It is defined as follows:

$$\psi = \frac{2\pi}{g}\int_0^P a\cos\varphi[v]dp \tag{4}$$

$$[v] = \frac{1}{2\pi}\int_0^{2\pi} v d\lambda \tag{5}$$

where g is the acceleration of gravity, p is the pressure, φ is the latitude, a is the radius of the Earth, v is the meridional velocity, and [ ] denotes the zonal mean.

The presumption of meridional circulation devoid of divergence holds true only at the global scale. This is because mass conservation is a global concept and not necessarily works regionally. Therefore, the regional Hadley circulation is defined by the vertical profiles of the zonally averaged meridional wind divergence and the vertical p-velocity within a specific regional domain (Sharmila & Walsh, 2018). In addition, we also use the vertical shear of meridional wind between 200 hPa and 850 hPa to determine the magnitude and meridional extent of the Hadley circulation following the previous study (Sun et al., 2017).

2.6. Signal-to-noise ratio and statistical significance

The noise denotes the natural climate variability and the signal denotes the climate change due to global warming. Thus, the signal-to-noise ratio tells when the climate change signal due to global warming overcomes the internal climate variability. Previous studies have used the outputs of global climate models to determine the time of emergence of the anthropogenic climate change signals in precipitation, surface air temperature, and SST change by using the signal-to-noise ratio (e.g., Giorgi and Bi, 2009; Hawkins and Sutton, 2012; Ying et al., 2022). Following the previous studies, we use the signal-to-noise ratio to estimate the time of emergence of TC genesis at higher latitudes in the specific regions. The signal is defined as the ensemble-mean TC genesis difference in HST minus NWA, W2K minus NWA, and W4K minus NWA. The noise is determined as the ensemble-mean standard deviation of TC genesis in NWA run. The time of emergence for poleward shift of TC genesis is estimated when the signal-to-noise ratio is higher than 1.

We assess the statistical significance of composite analysis through a two-tailed Student's *t*-test with a 95% confidence level.

3. Poleward shift of TC genesis at a global scale in large-ensemble simulations

To scrutinize the influence of different warming scenarios on TC genesis locations, we utilize the four ensembles of the d4PDF simulation: no-warming (NWA), historical warming (HST), +2 K warming (W2K), and +4 K warming (W4K) scenarios

(Supplementary Table 1). All analyses are predicated upon the ensemble mean. The results demonstrate a gradual decline in global TC genesis frequency from NWA to W4K (Supplementary Fig. 2), in line with prior studies (Sugi et al., 2002; Knutson et al., 2020; Zhao et al., 2009). The annual mean TC genesis number in NWA and W2K increases and decreases by 15% compared to that in HST (Supplementary Figs. 2b-d), respectively. In contrast, the annual mean TC genesis number in W4K decreases by 33% (Supplementary Figs. 2b, e). On average, there is a decrease (increase) of 11-15% in mean TC genesis number per 1 K warming (cooling) (Held & Zhao, 2011; Yoshimura & Sugi, 2005).

Analyzing the contrasts of TC genesis frequency during JASO and JFMA in the NWA, W2K, and W4K runs compared to the HST run, that is, HST-NWA, W2K-HST, and W4K-HST for brevity, reveals notable patterns. Specifically, TC genesis frequency decreases over the western North Pacific, Bay of Bengal, southern Indian Ocean, and southern Pacific Ocean (Fig. 1). Different features of TC genesis changes emerge over the northern Atlantic Ocean. The difference in TC genesis frequency in HST-NWA suggests an increase of TC genesis over the northern Atlantic Ocean (Fig. 1a). Conversely, the difference in W4K-HST indicates a decrease in TC genesis (Fig. 1c). The simulated increase in TC genesis in HST-NWA over the northern Atlantic Ocean is attributed to reduced aerosol concentrations over Europe and the United States (Murakami et al., 2020; Murakami, 2022). However, as global warming intensifies, the dominant effect of greenhouse gas concentrations results in a decreasing trend in TC genesis (Murakami,

2022).

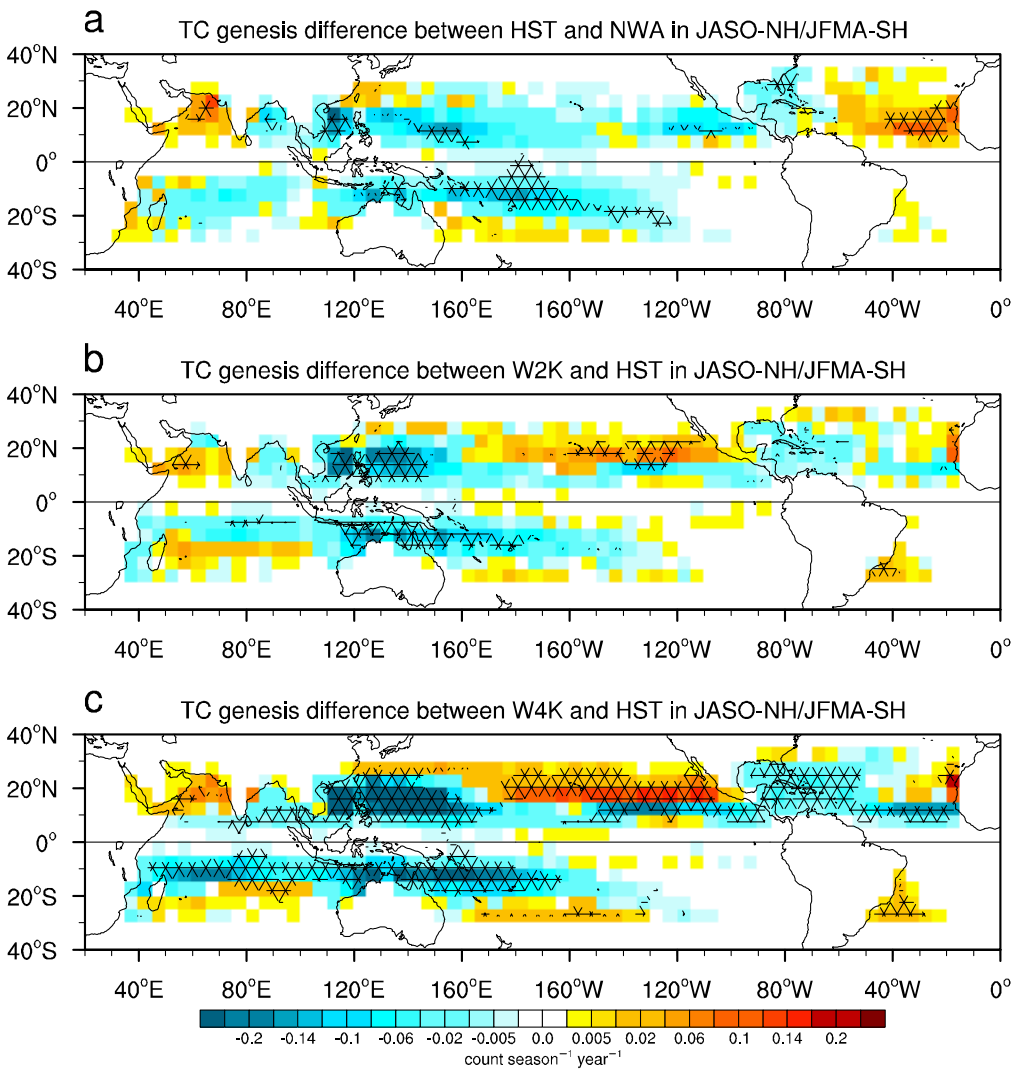

Figure 1. The contrast of TC genesis frequency between (a) HST and NWA, (b) W2K and HST, and (c) W4K and HST during JASO in NH and JFMA in SH. All the difference is defined as the former minus latter, implying the warming effect on the TC genesis frequency based on the 100-member d4PDF ensemble for 32 years. The cross-hatched region denotes that the difference in the TC genesis frequency is significant at the 95% confidence level.

In addition to the decrease in TC genesis over major TC regions, another prominent feature is a substantial rise in TC genesis at higher latitudes worldwide, except for the northern Atlantic Ocean in W4K-HST (Fig. 1c). This TC genesis increase at higher latitudes is also observed in W2K, though not as significant (Fig. 1b). The zonal-mean difference in TC genesis frequency reveals a decrease in TC genesis between 5°-20° latitudes and an increase between 20°-35° latitudes in both hemispheres (Figs. 2a and 2b), indicating a poleward migration in TC genesis location in a changing climate. It is worth emphasizing that the hemisphere-mean difference is subtracted in Figs. 2a and 2b to highlight the contrast of TC genesis change between low and high latitudes.

To further support this global pattern of the poleward migration in TC genesis, we further calculate the probability density function of TC genesis with latitude in JASO of NH and JFMA of SH (Fig. 2c and Fig. 2d). The results show that in latitudes equatorward of 15° in both hemispheres, the rate of TC genesis within each 5° range decreases with increasing global warming. In contrast, in latitudes poleward of 15° in both hemispheres, the rate of TC genesis increases from NWA to W4K (Figs. 2c and 2d). Notably, there is a poleward shift in the preferred latitude of TC genesis in NH, moving from 10°-15°N in NWA and HST to 15°-20°N in W2K and W4K (Fig. 2c). These histograms clearly indicate that more TCs are generated at higher latitudes under global warming.

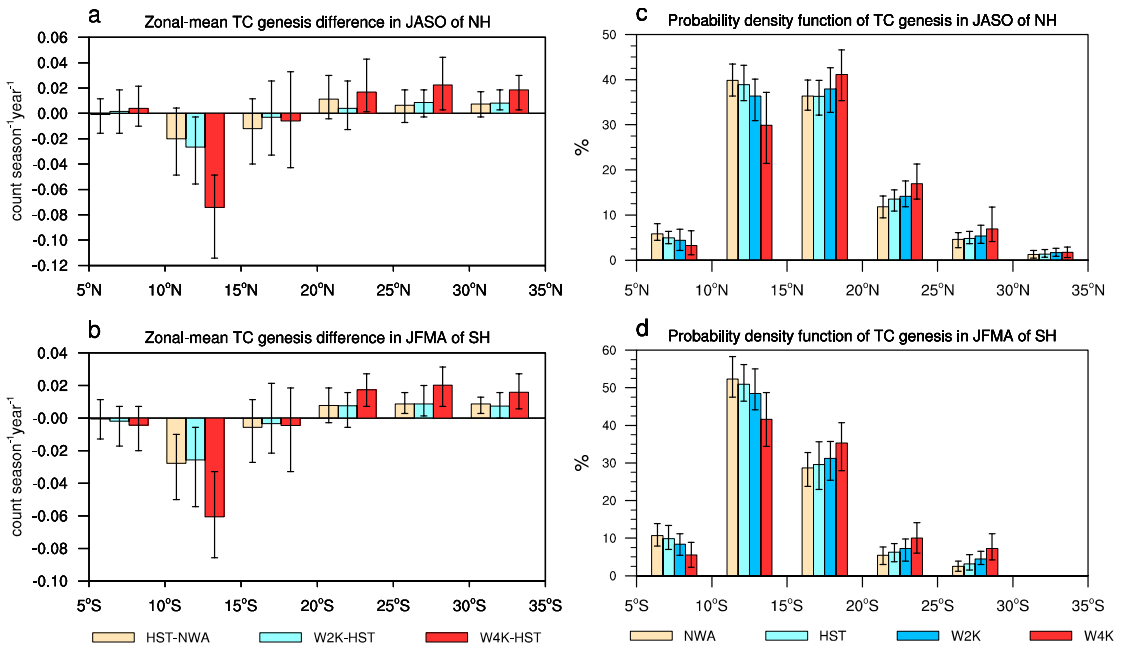

Figure 2. a, b, The distribution of TC genesis frequency difference between HST and NWA (light orange), W2K and HST (light blue), and W4K and HST (red) in a 5° latitudinal bin in (a) JASO in NH and (b) JFMA in SH. The hemisphere-mean (0-35°) difference has been removed. c, d, As in a, b, except for the probability distribution of TC genesis (in %) in the four experiments: NWA (light orange), HST (light blue), W2K (blue), and W4K (red). The error bars indicate the range from all members for each ensemble.

Upon calculating the meridional variations of TC genesis across the six TC active regions (Supplementary Fig. 1), a substantial decline in TC genesis at lower latitudes and an increase in TC genesis at higher latitudes are observed over the western North Pacific and eastern North Pacific during JASO as well as over the southern Pacific Ocean and southern Indian Ocean during JFMA (Supplementary Figs. 3a-b and Supplementary Figs.

311 3e-f). Simultaneously, a similar pattern is seen in the probability density function of TC
312 genesis with latitude across all ocean basins as that observed in both NH and SH (Figs.
313 2c-d and Supplementary Fig. 4). Remarkably, a distinct poleward migration in the peak
314 TC genesis region is noticeable over the northern Atlantic Ocean and southern Pacific
315 Ocean, transitioning from the 10 °-15 ° latitudes to the 15 °-20 ° latitudes as global warming
316 intensifies (Supplementary Figs. 4c, 4f), despite the lack of a clear increase in TC genesis
317 frequency at higher latitudes over the northern Atlantic Ocean in W4K-HST (Fig. 1c).

318 **4. Possible mechanisms underlying poleward shift of TC genesis at a global scale**

319 Previous studies attributed the decline of TC genesis frequency under climate
320 change to the increase of moist saturation deficit (Emanuel et al., 2008). Our analysis
321 indicates that changes in moist saturation deficit cannot explain the poleward shift of TC
322 genesis because the differences in moist saturation deficit in HST-NWA, W2K-HST, and
323 W4K-HST all display an increase around the globe, in particular significantly over the
324 subtropical regions (Supplementary Fig. 5). The increase in moist saturation deficit
325 indicates that the middle atmosphere is not favorable for TC genesis. Alternatively, a
326 recent observational study suggested that the poleward migration of TC genesis is
327 associated with the Hadley cell expansion (Sharmila & Walsh, 2018), which is also
328 examined here using the vertical profile of zonal-mean mass stream function that
329 quantifies the global Hadley cell width. Positive values denote a clockwise flow while
330 negative values indicate an anticlockwise flow. The difference in HST-NWA, W2K-HST,
331 and W4K-HST reveals that the Hadley cell expansion is weak in JASO of NH
332 (Supplementary Figs. 6a, c, e), whereas the SH displays a slight expansion
333 (Supplementary Figs. 6b, d, f). The meridional distribution of zonal-mean vertical

meridional wind shear between 200 hPa and 850 hPa supports the above findings (Supplementary Fig. 7). Thus, the Hadley cell expansion cannot solely explain the poleward migration of TC genesis, particularly in NH.

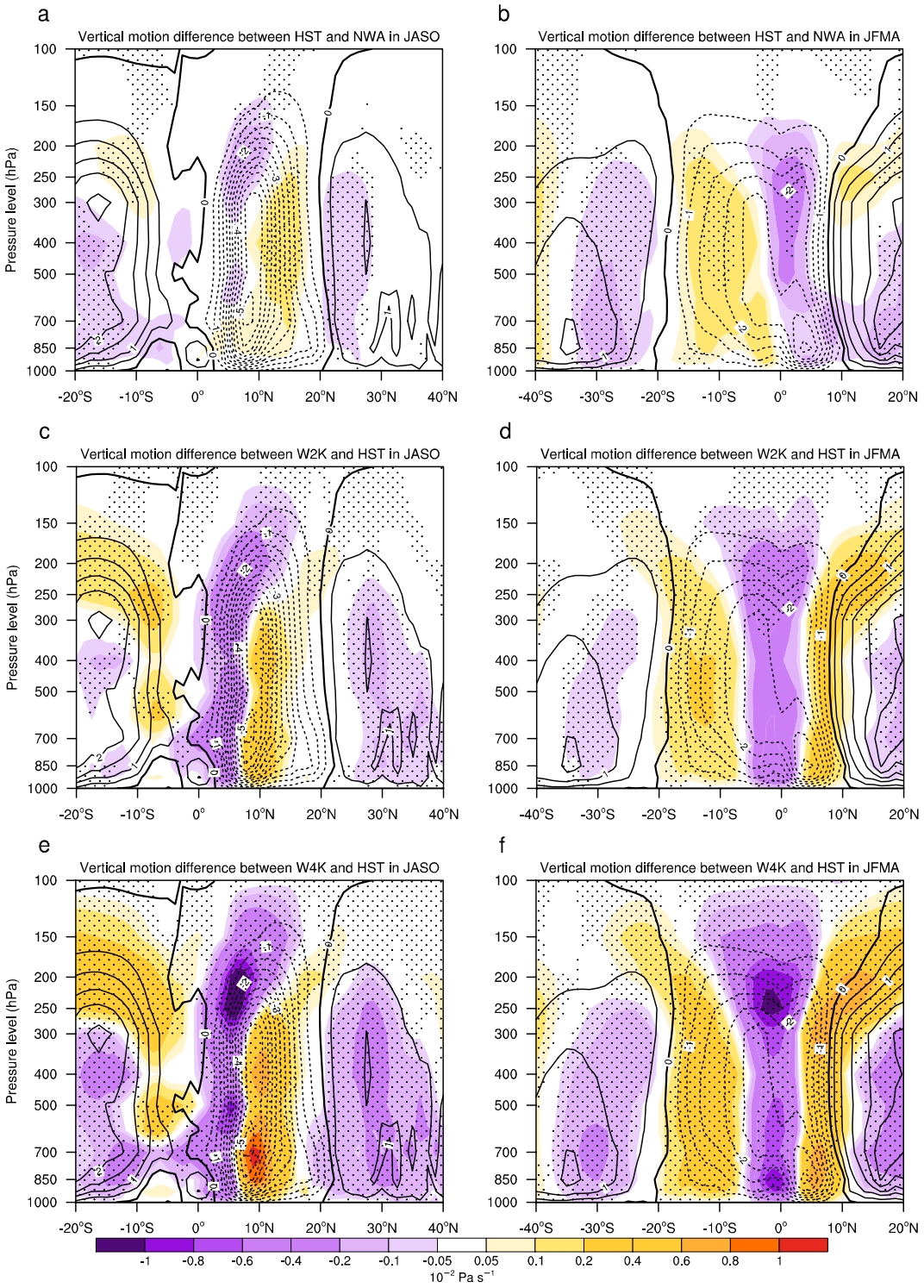

Figure 3. The difference of vertical p-velocity (ω, 10^{-2} Pa s^{-1}) during (left) JASO and (right) JFMA between (a-b) HST and NWA, (c-d) W2K and HST, and (e-f) W4K and HST. Positive values in reddish shading correspond to the anomalous downward motion and vice versa for negative values in purplish shading. The contour indicates the climatology of zonal-mean ω in HST during JASO and JFMA (dashed contour corresponding to the upward motion). The dotted areas denote that the difference is statistically significant at the 95% confidence level.

Interestingly, a weakening of the Hadley cell is seen from NWA to W4K in both hemispheres (Supplementary Figs. 6-7). As such, Fig. 3 directly shows an anomalous descending motion in the climatological mean rising branch of the Halley cell and an anomalous ascending motion in the climatological mean subsiding branch during JASO of NH and JFMA of SH, which indicates an apparent weakening of the Halley cell under a changing climate. This Hadley cell weakening may be associated with the increased vertical stability (Supplementary Fig. 8), as evidenced by the peak of positive equivalent potential temperature difference being at the upper troposphere around the tropics, which is in line with prior studies (Allen & Sherwood, 2008; Santer et al., 2005; Fu et al., 2011; Sugi et al., 2015). As global warming intensifies, the signals of anomalous descending motion in the tropics and ascending motion in the subtropics become stronger (Fig. 3).

In order to establish a link between other dynamical environmental factors and the reduction of TC genesis at lower latitudes and its increase at higher latitudes altogether leading to the poleward migration of TC genesis, we compare the difference in

zonal-mean low-level relative vorticity and upper-level divergence in HST-NWA, W2K-HST, and W4K-HST in JASO of NH and JFMA of SH as well as the climatological mean distribution in HST for reference (Fig. 4). Those two variables are known to be important factors for TC genesis (Cao et al., 2018, 2019). Our analysis reveals a harmonious agreement between the poleward shift of TC genesis and the meridional changes in low-level relative vorticity and upper-level divergence. Specifically, a decrease in low-level relative vorticity is present at lower latitudes and an enhancement occurs at higher latitudes (Fig. 4). Note that in SH, TC genesis is related to anticyclonic vorticity, and the sign of vorticity change is reversed (Figs. 4a-c).

Of particular interest is the meridional distribution of differences in the upper-level divergence, which perfectly matches the variations in the TC genesis. In both hemispheres, the reduction in TC genesis between 5 ° and 20 ° latitudes corresponds to a weakening of climatological upper-level divergence, while the increase in TC genesis between 20 ° and 35 ° latitudes corresponds to a weakening of climatological upper-level convergence (Figs. 4d-f and Figs. 2a-b). The changes in upper-level divergence are closely linked to the vertical p-velocity due to mass continuity, further highlighting their dominant roles in shaping the meridional distribution of TC genesis. Note that even though there is strengthened upper-level divergence and low-level relative vorticity between 5 ℃S and 5 ℃N (Fig. 4), the frequency of TC genesis does not increase due to the low planetary vorticity. In addition, we find that vertical wind shear, SST, and mid-level relative humidity is not tightly linked to the poleward shift of TC genesis, while the DGPI

can only explain the poleward shift of TC genesis in NH (Supplementary Fig. 9). This is because the DGPI in SH is dominantly by the vertical wind shear. The positive contribution from vertical pressure velocity and lower-level vorticity is overwhelmed by the negative contribution from vertical wind shear, which results in inconsistent changes in the DGPI and TC genesis location in SH.

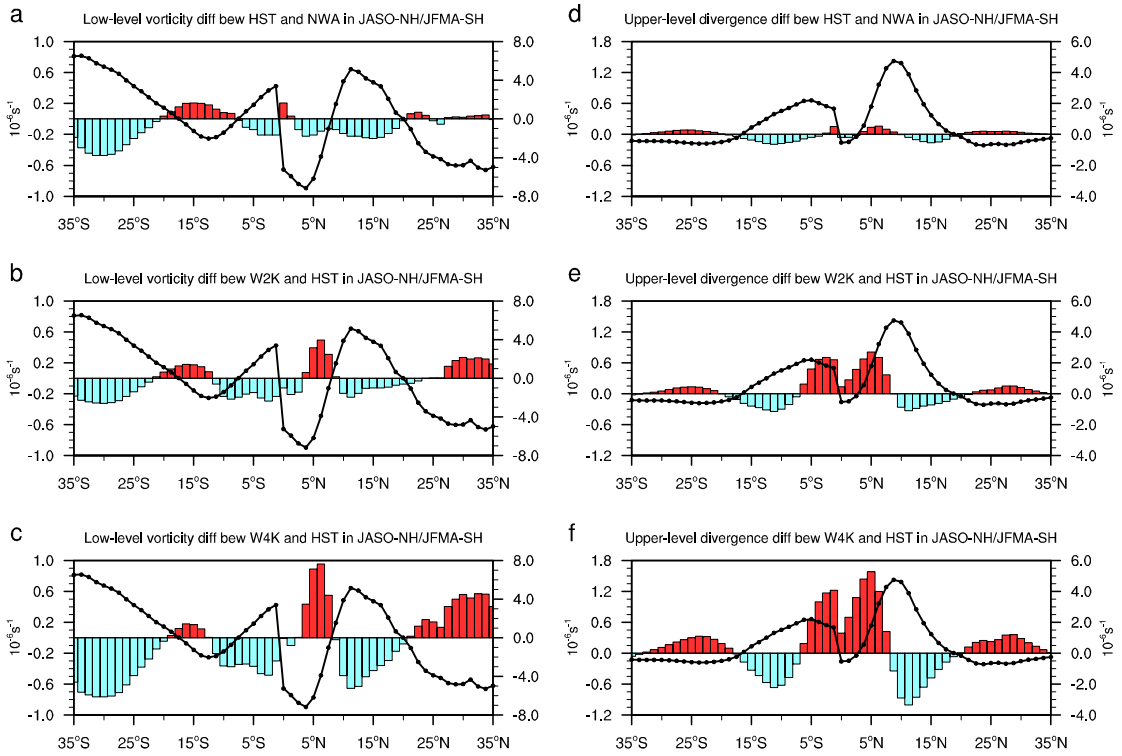

Figure 4. The zonal-mean distribution of the difference in (a-c) 850-hPa relative vorticity (10^{-6} s^{-1}) and (d-f) 200-hPa divergence (10^{-6} s^{-1}) during JASO in the Northern Hemisphere and JFMA in the Southern Hemisphere (the scale on the left). The difference is taken between (a, d) HST and NWA, (b, e) W2K and HST, and (c, f) W4K and HST. The solid line indicates the climatology of the zonal-mean (a-c) 850-hPa relative vorticity and (d-f) 200-hPa divergence in HST (the scale on the right).

It is important to acknowledge that the presumption of the meridional circulation devoid of divergence, as determined by mass stream function, may not hold true over the regional TC genesis domains. Thus, we employ the zonally averaged vertical profile of meridional wind divergence and vertical p-velocity within the specific domains to portray the regional Hadley circulation (Sharmila & Walsh, 2018). With increasing global warming, the regional Hadley cells exhibit weakening tendencies during the TC seasons in various basins (Supplementary Fig. 10 and Fig. 11), which are characterized by descending anomalies at lower latitudes and ascending anomalies at higher latitudes. Specifically, the widened ascending anomalies over the eastern North Pacific closely match with the significant enhancement in TC genesis north of 15 ℃N (Fig. 1c and Supplementary Fig. 10j). Conversely, the narrowing of the ascending anomalies over the northern Atlantic Ocean corresponds to the relatively insignificant increase in TC genesis at higher latitudes (Fig. 1c and Supplementary Fig. 10l). This pattern of weakening in the ascending and descending branches of the regional Hadley circulation aligns well with the anomalies of low-latitude convergence and high-latitude divergence at upper level within each basin (Supplementary Fig. 12).

Seo et al. (2014) suggested that the strength of the Hadley circulation is associated with three factors, including the meridional potential temperature gradient, gross static stability and tropopause height. Thus, we further examine the relationship between the change of Hadley circulation strength and the meridional potential temperature gradient at each basin under different global warming levels. The Hadley cell strength is measured as vertical pressure velocity at 500 hPa (-ω) in the subtropical region at each basin, while the meridional potential temperature gradient is defined as $\Delta_{PT} = \frac{\theta_{[10°S-10°N]} - \theta_{[10°N-50°N]}}{\theta_0}$

in NH and $\Delta_{PT} = \frac{\theta_{[10°S-10°N]} - \theta_{[10°S-50°S]}}{\theta_0}$ in SH, in which θ_0 denotes the hemispheric troposphere mean potential temperature (Seo et al., 2014). It is seen that the regional change in the Hadley circulation strength is negatively correlated with the regional change in the equator-to-high-latitude difference of potential temperature, which is significant at the 95% confidence level (Supplementary Fig. 13a). It indicates that a greater decline in the meridional potential temperature may result in the greater decline of the Hadley circulation strength (Seo et al., 2014; Sun et al., 2019).

Furthermore, the change in the Hadley circulation strength is positively correlated with the TC genesis difference in the subtropical region at each basin with the correlation coefficient as high as 0.8, which is significant at the 99% confidence level (Supplementary Fig. 13b). It denotes that anomalous high-latitude ascending motions at each basin are closely connected to the basin-specific variations in TC genesis (Fig. 1c). These findings are in broad accordance with the poleward migration in the anomalous large-scale atmospheric conditions favorable for TC genesis.

5. Time of emergence for the poleward shift of TC genesis

Regarding the potential implication of the poleward shift of TC genesis, we conduct an estimation of the time of emergence for the poleward shift of TC genesis by using the signal-to-noise ratio (Giorgi and Bi, 2009; Hawkins and Sutton, 2012). From the difference of TC genesis frequency in W4K-HST, six key regions are selected with significant increase of TC genesis over higher latitudes as shown in Supplementary Fig. 14. Note that the southern Atlantic Ocean is chosen due to substantial increase of TC

genesis under global warming though the climatological mean TC genesis is limited (Supplementary Fig. 1).

In d4PDF dataset, a “time slice” method is applied. Thus, we only use 3 samples (no warming, 2 K warming and 4 K warming) to perform linear regression analysis. Note that HST minus NWA represents 1 K warming level, W2K minus NWA represents 2 K warming level, and W4K minus NWA represents 4 K warming level. Based on the linear regression relationship, we estimate that the signal of TC genesis is likely to emerge over high latitudes of the Arabian Sea, southern Pacific Ocean, and southern Atlantic Ocean under 2 K warming and over high latitudes of the western North Pacific and eastern North Pacific under 4 K warming when the signal-to-noise ratio exceeds 1 (Fig. 5). It is noteworthy that there is a slight decrease of TC genesis in a narrow region north of 20 °N over the Arabian Sea in W2K-HST (Fig. 1b). However, when we select the Arabian Sea in the region of 10 °N-25 °N, 55 °E-75 °E (Supplementary Fig. 14), the signals in TC genesis have emerged from the noise of natural climate variability under 2 K warming.

Meantime, we further examine whether the time of emergence for the poleward shift of TC genesis is member-dependent (Supplementary Fig. 15). We calculate the signal-to-noise ratio of TC genesis frequency over the six key regions from 20, 30, 40 and 50 members with the members randomly selected. A notable difference is seen in the southern Atlantic Ocean. The signal of TC genesis appears over the southern Atlantic Ocean under 4 K warming, particularly, for 20, 30, and 50 members (Supplementary Figs.

15a, 15b, and 15d). The time of emergence for the poleward shift of TC genesis in other basins is not so sensitive to the number of selected members.

The estimation of time of emergence for the poleward shift of TC genesis is dependent on the rate between the signals of climate change and the noise of natural climate variability. Examination of relative magnitudes of signal and noise indicates that there are large natural climate variabilities over the western and eastern North Pacific, which delays the time of emergence for the TC genesis over the high latitudes, whereas over the southern Pacific Ocean and southern Atlantic Ocean, the signals in TC genesis emerge earlier due to relatively low natural climate variabilities. For the Arabian Sea, the signals in TC genesis are obviously great under 2 K warming. These results imply that the potential risks associated with TC-related hazards at higher latitudes will be heightened as global warming is higher than 2 K.

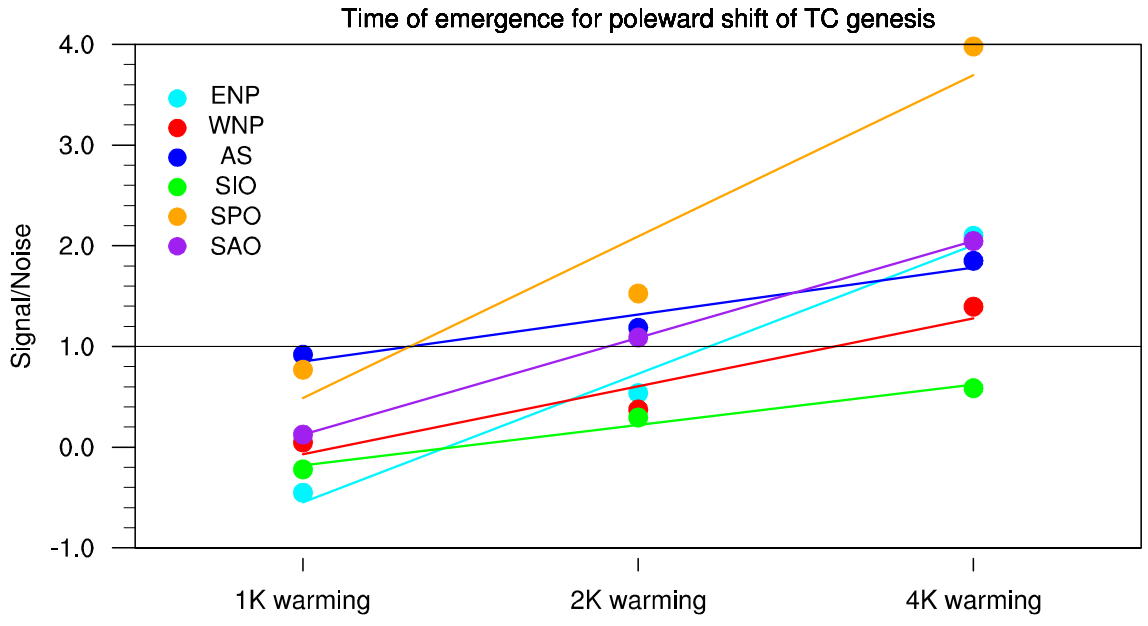

Figure 5. The signal-to-noise ratio of TC genesis frequency over the six key regions (Supplementary Fig. 13). The colored solid line denotes the linear regression. The signal is defined as the TC genesis difference in HST-NWA (global warming level of 1 K), W2K-NWA (2 K), and W4K-NWA (4 K).

6. Summary and discussion

Our findings emphasize a potentially new dynamical connection between the weakening of the Hadley cell and the robust poleward shift of TC genesis under the future 4 K warming scenario. This possible linkage is summarized in a schematic diagram (Supplementary Fig. 16). While our findings demonstrate regional disparities, most basins indicate a decline of TC genesis at low latitudes, an increase at high latitudes, and thus a poleward shift in TC genesis latitude. These variations are tightly connected to the dynamics of the weakened regional Hadley circulation, which exerts a suppressing effect on TC genesis at low latitudes and an enhancing effect at high latitudes. This weakening of Hadley circulation is possibly connected to the larger warming of the upper levels and the consequent increase in vertical stability (Sugi et al., 2002; Knutson & Manabe, 1995). Therefore, the perspective of the Hadley circulation intensity change integrates both the large-scale dynamic and thermodynamic conditions influencing regional TC genesis frequency. It offers a new framework to understand how future changes in TC genesis location occur through the weakening of meridional circulation caused by global

warming. Although the weakened descending motion does not mean a change in the direction of mean vertical motion, it indicates an increase in the ascending motion anomalies and thus the variance of synoptic-scale disturbances, which is favorable for more TC geneses at higher latitudes. Previous studies (Li et al., 2010; Murakami et al., 2012b) have attributed the TC genesis shift to the variance of synoptic-scale disturbances, which originate from the enhancement of upward motion anomalies in the predominantly subsiding branch over the central Pacific. In the future, we will analyze the daily data to inspect the changes in the synoptic scale activity in order to validate our hypothesis.

Previous studies have projected a poleward expansion of the global Hadley circulation during the twenty-first century using ensemble climate models from the Coupled Model Intercomparison Project phase 5/6 (CMIP5/6) under global warming (Sharmila & Walsh, 2018; Hu et al., 2013, 2018; Grise & Davis, 2020). However, the simulated poleward expansion in CMIP5 models is considerably weaker than that observed in reanalysis data (Hu et al., 2013, 2018). In our analysis of the large-ensemble d4PDF dataset, the tropical expansion alone is insufficient to explain the poleward migration of TC genesis around the globe. In line with previous climate models (Chemke & Yuval, 2023; Held & Soden, 2006; Hu et al., 2018; Knutson & Manabe, 1995; Lu et al., 2007), a future weakening of the global Hadley circulation strength will likely occur in response to global warming. When the fractional change of precipitation is smaller than that of boundary layer mixing ratio, the upward convective mass flux and the

compensating subsidence both decrease (Held & Soden, 2006). This suggests that the poleward shift of TC genesis is intimately related to the weakening of meridional circulation. Further analysis is warranted to better comprehend the relationship between the reduction of upward (downward) mass flux and the decrease (increase) of TC genesis at low (high) latitudes (Sugi et al., 2012). In addition, previous studies have used climate modes included in CMIP6 HighResMIP to examine the projections of TC genesis frequency under global warming (e.g., Yamada et al., 2021). However, their results do not project a clear poleward shift of TC genesis. This source of uncertainty may be due to model resolutions, simulation settings, and ensemble members. In the future, we will use different models with higher resolution and more members to validate the obtained results in the present study.

Changes of TC genesis are closely linked to variations in TC occurrence (track). A significant decrease in TC occurrence appears over the western North Pacific, southern Pacific Ocean, southern Indian Ocean, and the western portion of northern Atlantic Ocean in W4K-HST (Supplementary Fig. 17c). However, a prominent increase in TC occurrence is seen over the central North Pacific (north of 10 °N), the northeastern section of northern Atlantic Ocean, the southern Atlantic Ocean (south of 15 °S), the Arabian Sea (north of 15 °N) and the northeastern region of China in W4K-HST (Supplementary Fig. 17c). Some features of TC occurrence in the context of climate change accord with prior findings (Murakami et al., 2017; Yoshida et al., 2017), which indicate that there is a

propensity for TC activity to shift towards higher latitudes as global warming intensifies (Knutson et al., 2020). Consequently, our results highlight the potential for increased TC-related hazards at higher latitudes due to ongoing global warming (Studholme et al, 2022). Meantime, the decrease of TC genesis and occurrence at lower latitudes implies that future climate warming may exacerbate drought conditions in mainland areas worldwide (Yuan et al., 2023). This enhanced understanding of the influence of a changing climate on TC activity provides valuable insights for policymakers and stakeholders in their endeavors to effectively mitigate and adapt to the impacts of global warming.

Acknowledgments

We appreciate the comments from two reviewers which significantly enhance the quality of this paper. X.C. appreciates Miki Arai for helping download the d4PDF data and Prof. Feifei Jin from University of Hawaii and Dr. Yong Sun for the valuable suggestions. X.C. was supported by the National Natural Science Foundation of China (Grants 42025503, 42130608, 41721004), the State Key Laboratory of Tropical Oceanography, South China Sea Institute of Oceanology, Chinese Academy of Sciences (Project No. LTO2203), the Open Grants of the State Key Laboratory of Severe Weather (Grant 2022LASW-B03), and the China Scholarship Council. M.W. was supported by the Program for Advanced Studies of Climate Change Projection (SENTAN) Grant-in-Aid JPMXD0722680395

549 from the Ministry of Education, Culture, Sports, Science and Technology (MEXT), Japan.
550 L.W. was supported by the National Natural Science Foundation of China (Grant
551 42175050), the Youth Innovation Promotion Association (CAS Y2021030).

552 **Open Research**

553 **Data and code availability statement**

554 The data supporting the findings of the present study are openly available. The IBTrACS
555 data were obtained from the following website:
556 https://www.ncei.noaa.gov/data/international-best-track-archive-for-climate-stewardship-i
557 btracs/v04r00/access/netcdf/. The d4PDF dataset can be accessed at
558 http://d4pdf.diasjp.net/d4PDF.cgi?target=GCM&lang=en. The TC track dataset in d4PDF
559 is available from https://data.diasjp.net/dl/storages/filelist/dataset:640 and
560 https://climate.mri-jma.go.jp/pub/d4pdf/tropical_cyclone_tracks/. Note that the d4PDF
561 dataset and TC track dataset in d4PDF require a registration to access them.
562

References

Allen, M. R. & Ingram, W. J. (2002). Constraints on future changes in climate and the hydrologic cycle. *Nature*, **419**, 224-232.

Allen, R. J. & Sherwood, S. C. (2008). Warming maximum in the tropical upper troposphere deduced from thermal winds. *Nat. Geosci.*, **1**, 399-403.

Bhatia, K. et al. (2018). Projected response of tropical cyclone intensity and intensification in a global climate model. *J. Clim.*, **31**, 8281-8303.

Cao, X., Wu, R. & Bi, M. (2018). Contributions of different time-scale variations to tropical cyclogenesis over the western North Pacific. *J. Clim.* **31**, 3137-3153.

Cao, X. et al. (2019). Contribution of different time-scale variations to the tropical cyclogenesis environment over the northern tropical Atlantic and comparison with the western North Pacific. *J. Clim.*, **32**, 6645-6661.

Chemke, R. & Yuval, J. (2023). Human-induced weakening of the Northern Hemisphere tropical circulation. *Nature*, **617**, 529-532.

Daloz, A. S. & Camargo, S. J. (2018). Is the poleward migration of tropical cyclone maximum intensity associated with a poleward migration of tropical cyclone genesis? *Clim. Dy.*, **50**, 705-715.

Deser, C., Knutti, R., Solomon, S., & Phillips, A. S. (2012). Communication of the role of natural variability in future North American climate, *Nat. Climate Change*, **2**, 775–779.

583 Emanuel, K. A. (2013). Downscaling CMIP5 climate models shows increased tropical
584 cyclone activity over the 21st century. *Proc. Natl Acad. Sci. USA*, **110**,
585 12219-12224.
586 Emanuel, K., Sundararajan, R. & Williams, J. (2008). Hurricanes and global warming:
587 results from downscaling IPCC AR4 simulations. *Bull. Am. Meteorol. Soc.*, **89**,
588 347-368.
589 Emanuel, K. A., & Nolan, D. S., 2004: Tropical cyclone activity and global climate.
590 *Preprints of 26th Conf. on Hurricanes and Tropical Meteorology,* Miami, FL, Amer.
591 Meteor. Soc., 240–241.
592 Fu, Q., Manabe, S. & Johanson, C. M. (2011). On the warming in the tropical upper
593 troposphere: models versus observations. *Geophys. Res. Lett.*, **38**, L15704.
594 Fujita, M. et al. (2019). Precipitation changes in a climate with 2-K surface warming
595 from large ensemble simulations using 60-km global and 20-km regional
596 atmospheric models. *Geophys. Res. Lett.*, **46**, 435-442.
597 Grise, K. M. & Davis, S. M. (2020). Hadley cell expansion in CMIP6 models. *Atmos.*
598 *Chem. Phys.*, **20**, 5249-5268.
599 Giorgi, F., & Bi, X. (2009). Time of emergence (TOE) of GHG-forced precipitation
600 change hot-spots, *Geophys. Res. Lett.*, 36, L06709.
601 Hawkins, E., & Sutton, R. (2012). Time of emergence of climate signals, *Geophys. Res.*
602 *Lett.*, 39, L01702.Haugen, M. A., Stein, M. L., Moyer, E. J., & Sriver, R. L. (2018).

603 Estimating Changes in Temperature Distributions in a Large Ensemble of Climate
604 Simulations Using Quantile Regression, *J. Climate*, **31**, 8573–8588.
605 Held, I. M. & Soden, B. J. (2006). Robust responses of the hydrological cycle to global
606 warming. *J. Clim.*, **19**, 5686-5699.
607 Held, I. M. & Zhao, M. (2011). The response of tropical cyclone statistics to an increase
608 in CO2 with fixed sea surface temperatures. *J. Clim.*, **24**, 5353-5364.
609 Hirahara, S., Ishii, M. & Fukuda, Y. (2014). Centennial-scale sea surface temperature
610 analysis and its uncertainty. *J. Clim.*, **27**, 57-75.
611 Hu, Y., Tao, L. & Liu, J. (2013). Poleward expansion of the hadley circulation in CMIP5
612 simulations. *Adv. Atmos. Sci.*, **30**, 790-795.
613 Hu, Y., Huang, H. & Zhou, C. (2018). Widening and weakening of the Hadley circulation
614 under global warming. *Sci. Bull.*, **63**, 640-644.
615 Kamae, Y. et al. (2017). Atmospheric rivers over the northwestern Pacific: climatology
616 and interannual variability. *J. Clim.*, **30**, 5605-5619.
617 Knapp, K. R. et al. (2010). The International Best Track Archive for Climate Stewardship
618 (IBTrACS): unifying tropical cyclone data. *Bull. Am. Meteorol. Soc.*, **91**, 363-376.
619 Knutson, T. R. & Manabe, S. (1995). Time-mean response over the tropical Pacific to
620 increased CO2 in a coupled ocean-atmosphere model. *J. Clim.*, **8**, 2181-2199.
621 Knutson, T. R. et al. (2010). Tropical cyclones and climate change. *Nat. Geosci.*, **3**,
622 157-163.

623 Knutson, T. R. et al. (2015). Global projections of intense tropical cyclone activity for the
624 late twenty-first century from dynamical downscaling of CMIP5/RCP4.5
625 scenarios. *J. Clim.* **28**, 7203-7224.
626 Knutson, T. et al. (2020). Tropical cyclones and climate change assessment: Part II:
627 projected response to anthropogenic warming. *Bull. Am. Meteorol. Soc.*, **101**,
628 E303-E322.
629 Kossin, J. P., Emanuel, K. A. & Camargo, S. J. (2016). Past and projected changes in
630 western North Pacific tropical cyclone exposure. *J. Clim.*, **29**, 5725-5739.
631 Lu, J., Vecchi, G. A. & Reichler, T. (2007). Expansion of the Hadley cell under global
632 warming. *Geophys. Res. Lett.*, **34**, L06805.
633 Li, T. et al. (2010).Global warming shifts Pacific tropical cyclone location. *Geophys. Res.*
634 *Lett.*, **37**, L21804.
635 Li, Z. et al. (2013). Bimodal character of cyclone climatology in the Bay of Bengal
636 modulated by monsoon seasonal cycle. *J. Clim.*, **26**, 1033-1046.
637 Maher, N., Milinski, S., & Ludwig, R. (2021). Large ensemble climate model simulations:
638 introduction, overview, and future prospects for utilising multiple types of large
639 ensemble, *Earth Syst. Dynam.*, 12, 401–418.Mei, W. & Li, S. (2022). Variability
640 and predictability of basinwide and sub-basin tropical cyclone genesis frequency
641 in the northwest Pacific. *J. Clim.*, **35**, 3265-3284.
642 Milinski, S., Maher, N., & Olonscheck, D. (2020). How large does a large ensemble need

643 to be? *Earth Syst. Dynam.*, 11, 885–901.
644 Mizuta, R. et al. (2017). Over 5,000 years of ensemble future climate simulations by
645 60-km global and 20-km regional atmospheric models. *Bull. Am. Meteorol. Soc.*,
646 **98**, 1383-1398.
647 Murakami, H. (2022). Substantial global influence of anthropogenic aerosols on tropical
648 cyclones over the past 40 years. *Sci. Adv.*, **8**, eabn9493.
649 Murakami, H., Mizuta, R. & Shindo, E. (2012a). Future changes in tropical cyclone
650 activity projected by multi-physics and multi-SST ensemble experiments using
651 the 60-km-mesh MRI-AGCM. *Clim. Dyn.*, **39**, 2569-2584.
652 Murakami, H., and Coauthors, (2012b). Future changes in tropical cyclone activity
653 projected by the new high-resolution MRI-AGCM. *J. Climate*, 25, 3237–3260.
654 Murakami, H., Vecchi, G. A. & Underwood, S. (2017). Increasing frequency of extremely
655 severe cyclonic storms over the Arabian Sea. *Nat. Clim. Change*, **7**, 885-889.
656 Murakami, H. et al. (2020). Detected climatic change in global distribution of tropical
657 cyclones. *Proc. Natl Acad. Sci. USA*, **117**, 10706-10714.
658 Nakamura, J. et al. (2017). Western North Pacific tropical cyclone model tracks in present
659 and future Climates. *J. Geophys. Res. Atmos.*, **122**, 9721-9744.
660 Santer, B. D. et al. (2005). Amplification of surface temperature trends and variability in
661 the tropical atmosphere. *Science*, **309**, 1551-1556.
662 Seneviratne, S. I. et al. (2021). Weather and climate extreme events in a changing climate.

In climate change 2021: the physical science basis. Contribution of working group I to the sixth assessment report of the Intergovernmental Panel on Climate Change. Cambridge University Press, pp 1513-1766.

Seo, K.-H., Frierson, D. M. W., & Son, J.-H. (2014). A mechanism for future changes in Hadley circulation strength in CMIP5 climate change simulations, *Geophys. Res. Lett.*, **40**, 5251–5258.

Sharmila, S. & Walsh, K. J. E. (2018). Recent poleward shift of tropical cyclone formation linked to Hadley cell expansion. *Nat. Clim. Change*, **8**, 730-736.

Sobel, A. H. et al. (2016). Human influence on tropical cyclone intensity. *Science*, **353**, 242-246.

Studholme, J. et al. (2022). Poleward expansion of tropical cyclone latitudes in warming climates. *Nat. Geosci.*, **15**, 14-28

Sugi, M., Murakami, H. & Yoshimura, J. (2009). A reduction in global tropical cyclone frequency due to global warming. *SOLA*, **5**, 164-167.

Sugi, M., Yoshida, K. & Murakami, H. (2015). More tropical cyclones in a cooler climate? *Geophys. Res. Lett.*, **42**, 6780-6784.

Sugi, M., Noda, A. & Sato, N. (2002). Influence of the global warming on tropical cyclone climatology: an experiment with the JMA global model. *J. Meteorol. Soc. Jpn. II*, **80**, 249-272.

Sugi, M., Murakami, H. & Yoshimura, J. (2012). On the mechanism of tropical cyclone

683 frequency changes due to global warming. *J. Meteorol. Soc. Jpn. II*, **90A**,
684 397-408.
685 Sun, Y., Zhou, T. & Wu, B. (2017). Simulation of long-term trends in Hadley circulation
686 during boreal winter using an ocean data assimilation scheme with the coupled
687 general circulation model FGOALS-s2. *Chin. Sci. Bull.* , **63**, 452-460.
688 Sun, Y. et al. (2019). Regional meridional cells governing the interannual variability of
689 the Hadley circulation in boreal winter. *Clim Dyn.*, **52**, 831–853.
690 Tory, K. J. et al. (2013). Projected changes in late-twenty-first-century tropical cyclone
691 frequency in 13 coupled climate models from phase 5 of the Coupled Model
692 Intercomparison Project. *J. Clim.*, **26**, 9946-9959.
693 Ueda, H., Miwa, K. & Kamae, Y. (2018). Seasonal modulation of tropical cyclone
694 occurrence associated with coherent Indo-Pacific variability during decaying
695 phase of El Niño. *J. Meteorol. Soc. Jpn. II*, **96**, 381-390.
696 Wang, B. & Murakami, H. (2020). Dynamic genesis potential index for diagnosing
697 present-day and future global tropical cyclone genesis. *Environ. Res. Lett.*, **15**,
698 114008.
699 Wang, Chao, Wang, Y. R, Wang, B., Wu, L. G., Zhao, H. K., & Cao, J. (2023). Opposite
700 skills of ENGPI and DGPI in depicting decadal variability of tropical cyclone
701 genesis over the western North Pacific, *J. Clim.*, doi: 10.1175/JCLI-D-23-0201.1.
702 Wehner, M. F. et al. (2018). Changes in tropical cyclones under stabilized 1.5 and 2.0 °C

703 global warming scenarios as simulated by the Community Atmospheric Model
704 under the HAPPI protocols. *Earth Syst. Dynam.*, **9**, 187-195.
705 Yamada, Y. et al. (2021). Evaluation of the contribution of tropical cyclone seeds to
706 changes in tropical cyclone frequency due to global warming in high-resolution
707 multi-model ensemble simulations. *Prog Earth Planet Sci*, **8**, 11.
708 Yan, Q., Korty, R., Zhang, Z. & Wang, H. (2019). Evolution of tropical cyclone genesis
709 regions during the Cenozoic era. *Nat. Commun.*, **10**, 3076.
710 Ying, J., et al. (2022). Emergence of climate change in the tropical Pacific. *Nat. Clim.*
711 *Chang*. 12, 356–364.
712 Yoshida, K. et al. (2017). Future changes in tropical cyclone activity in high-resolution
713 large-ensemble simulations. *Geophys. Res. Lett.*, **44**, 9910-9917.
714 Yoshimura, J. & Sugi, M. (2005). Tropical cyclone climatology in a high-resolution
715 AGCM −impacts of SST warming and CO2 increase−. *SOLA*, **1**, 133-136.
716 Yuan, X. et al. (2023). A global transition to flash droughts under climate change. *Science*,
717 **380**, 187-191.
718 Zhao, M., Held, I. M., Lin, S.-J. & Vecchi, G. A. (2009). Simulations of global hurricane
719 climatology, interannual variability, and response to global warming using a
720 50-km resolution GCM. *J. Clim.*, **22**, 6653-6678.
721 Zhao, M. et al. (2013). Robust direct effect of increasing atmospheric CO2 concentration
722 on global tropical cyclone frequency: a multi-model inter-comparison. *Us Clivar*

723 *Variations*, **11**, 17-23.